RESEARCH ARTICLE

A novel phosphoprotein analysis scheme for assessing changes in premalignant and malignant breast cell lines using 2-D liquid separations, protein microarrays, and tandem mass spectrometry

Tasneem H. Patwa[1], Yanfei Wang[1], Fred R. Miller[2], Steve Goodison[3], Subramaniam Pennathur[4], Timothy J. Barder[5] and David M. Lubman[1, 6, 7]

[1] Department of Chemistry, University of Michigan, Ann Arbor, MI, USA
[2] Department of Pathology, Barbara Ann Karmanos Cancer Institute, Wayne State University School of Medicine, Detroit, MI, USA
[3] Department of Surgery, University of Florida, Jacksonville, FL, USA
[4] Department of Internal Medicine, Division of Nephrology, University of Michigan Medical Center, Ann Arbor, MI, USA
[5] Eprogen Inc., Darien, IL, USA
[6] Department of Surgery, University of Michigan Medical Center, Ann Arbor, MI, USA
[7] Comprehensive Cancer Center, University of Michigan Medical Center, Ann Arbor, MI, USA

Received: April 25, 2008
Revised: May 28, 2008
Accepted: June 11, 2008

An analysis of phosphorylation changes that occur during cancer progression would provide insights into the molecular pathways responsible for a malignant phenotype. In this study we employed a novel coupling of 2-D liquid separations and protein microarray technology to reveal changes in phosphoprotein status between premalignant (AT1) and malignant (CA1a) cell lines derived from the human MCF10A breast cell lines. Intact proteins were first separated according to their p*I* and hydrophobicities, then arrayed on SuperAmine glass slides. Phosphoproteins were detected using the universal, inorganic phospho-sensor dye, Pro-Q Diamond. Using this dye, out of 140 spots that were positive for phosphorylation, a total of 85 differentially expressed spots were detected over a pH range of 7.2–4.0. Proteins were identified and their peptides sequenced by MS. The strategy enabled the identification of 75 differentially expressed phosphoproteins, from which 51 phosphorylation sites in 27 unique proteins were confirmed. Interestingly, the majority of differentially expressed phosphorylated proteins observed were nuclear proteins. Three regulators of apoptosis, Bad, Bax, and Acinus, were also differentially phosphorylated in the two cell lines. Further development of this strategy will facilitate an understanding of the mechanisms involved in malignancy progression and other disease-related phenotypes.

Keywords:
Breast cancer / Liquid chromatography / Phosphorylation / Protein microarray / Tandem mass spectrometry

Correspondence: Dr. David M. Lubman, Department of Surgery, The University of Michigan Medical Center, MSRB1, Rm A510B, 1150 West Medical Center Drive, Ann Arbor, MI 48109-0656, USA
E-mail: dmlubman@umich.edu
Fax: +1-734-615-2088

Abbreviations: CF, chromatofocusing; **EB,** elution buffer; **NPS,** nonporous silica; **SB,** start buffer

1 Introduction

Breast cancer is the most frequently diagnosed cancer in women. More than 200 000 new cases of breast cancer, with over 41 000 deaths, were expected in the United States in 2008 [1]. Breast cancer related deaths have declined by approximately 2.3% from 1990 to 2002 primarily due to earlier detection awareness as well as improved treatment. While

the five-year survival rate has increased to 98% for local-regional disease, it is only 26% for women with distant metastases [1]. Understanding the molecular mechanisms that underlie breast cancer development and progression to malignancy may uncover better therapeutic targets with potential utility to further decrease breast cancer mortality.

Aberrations in cellular signaling pathways have been associated with cancer development and progression, as cancer cell survival and proliferation rates increase, and as cancer cells become increasingly evasive to the immune system [2–4]. Growth factor signals are propagated from the cell surface intracellular milieu by signaling pathways, involving a variety of kinases such as membrane receptor kinases (EGFR, VEGF) and cytoplasmic kinases (ERK, MEK, Ras, PI3-K, and mTOR) [5]. In cancer, these signaling pathways are often dysregulated, resulting in a phenotype characterized by unfettered cell growth and increased invasive potential. Cellular signaling is largely controlled by transient, PTMs of signaling proteins, which alter their ability to bind and interact with downstream effectors [4–6]. Protein phosphorylation is one such modification that primarily acts as a molecular switch to activate or deactivate cellular signaling cascades [4, 7, 8]. A recent review by Krueger *et al.* [9] lists several phosphorylated proteins that are known to contribute to oncogenesis or are used in the context of a cancer biomarker. Proteins from all cellular compartments are represented in this list including histones, HDACs, MAP kinases, Akt, PTEN, EGFRs, and ILK.

A variety of techniques have been used to study phosphorylation expression on a large scale [10, 11]. One such technique involves incubation of cells with radioactive ^{32}P followed by 2-DE [12]. Although able to detect a wide dynamic range of phosphoproteins, this method requires handling of radioactive orthophosphate which makes it less favorable. In addition, the dependence on turnover rates at which the orthophosphate is incorporated into proteins may reduce sensitivity of this technique. The use of monoclonal and polyclonal antibodies specific to phosphorylated proteins to detect global phosphoprotein patterns on gels [13] circumvents the use of radiolabels. However, current available phosphoserine-specific and phosphothreonine-specific antibodies are not always reliable and cannot detect phosphoproteins where steric hindrance prevents antibody binding. More recently, a novel small molecule phosphosensor dye has been reported for detecting phosphoproteins on both gel and microarray platforms [14–17]. This dye is able to detect phosphotyrosine, serine, and threonine residues and can discriminate between thiophosphorylation and sulfation.

Gel-based methods have been considered the method of choice in studying global protein expression, but more recently developed techniques have focused on liquid-based methods due to the ease of coupling to mass spectrometers for protein identification [18–21]. The liquid-based method most frequently used for phosphoprotein analysis in complex samples involves shotgun proteomics where a complex protein mixture is first digested and enriched for phosphopeptides [22–24]. An enrichment step is often necessary since phosphopeptide ionization is typically suppressed in the presence of many nonphosphorylated peptides present in a complex sample. The enriched peptides are then analyzed by LC-MS/MS with comprehensive database searching to confirm identity and elucidate the phosphorylation site. A variety of enrichment methods have been developed ranging from immobilized metal affinity chromatography [25, 26] to amphoteric oxide-based enrichment, frequently using titanium or zirconium dioxide [27], as well as antibody-based enrichment. While shotgun proteomics is a high-throughput method at the experimental front, it is very time-consuming at the analysis end since data must be closely examined for possible false positives and negatives [28].

To overcome some of these limitations, we have been developing the coupling of comprehensive 2-D liquid separation methods to protein microarray technology. Performance evaluation of arrays generated from 2-D liquid separations has been reported elsewhere [29]. We have used this combined liquid separation and protein microarray strategy previously to assess the phosphorylation status of all proteins in a cell line that was treated with a specific protein kinase inhibitor [30]. While that study was successful in highlighting phosphorylation changes caused by experimentally perturbing a specific biological pathway, there are currently no reports investigating such changes in naturally occurring disease states. A study comparing phosphorylation status in disease states may have utility in elucidation of pathways that play a role in the progression of the disease.

A xenograft model of human breast disease progression has been developed from the MCF10A breast epithelial cell lines. Selected cell lines within the series are representative of normal, premalignant, and malignant phenotypes [31–33]. T24 c-Ha-ras oncogene-transfected MCF10A cells (MCF10A-neoT) form small, flat nodules in Nude/Beige mice which persist for the life span of the host and sporadically progress to carcinomas. A variant cell line (MCF10AT1), derived from one xenograft, not only forms simple differentiated ducts which persist in xenografts and sporadically progress to carcinoma, but also forms intermediate proliferative lesions resembling proliferative disease without atypia, atypical hyperplasia, and carcinoma *in situ*. By establishing cells in culture representing different stages in progression of MCF10AT through atypical hyperplasia to carcinoma, interruption of progression has been made possible. These cell lines continue to progress when reimplanted *in vivo* in immune deficient mice but are sufficiently stable *in vitro* to provide the tools essential for the genetic analysis of progression. MCF10AT cells express low levels of estrogen receptor (ER) and estradiol (E2) accelerates progression of the premalignant xenograft lesions. Fully malignant variants (MCF10CA lines), some of which are metastatic have also been recently derived.

In this study, we compared the phosphoproteome of premalignant (MCF10AT1) and malignant (MCF10CA1a c11) cell lines using a 2-D liquid-phase separation method

coupled to protein microarray technology. These two cell lines were chosen because they represent the initial (premalignant) and final (malignant, metastatic) stages of breast disease. The naturally occurring, arrayed proteins were probed with the small-molecule phosphosensor dye, Pro-Q Diamond, and antiphosphotyrosine antibodies. The strategy enabled us to detect and identify differentially expressed phosphoproteins and to determine specific changes associated with the premalignant and malignant phenotypes.

2 Materials and methods

2.1 Sample preparation

2.1.1 Cell lines

The premalignant AT1 cell line (MCF10AT1) and malignant CA1a cell line (MCF10CA1a c11) were both derived from the MCF10A human breast cell line and were maintained and prepared as previously described [31, 33].

2.1.2 Cell lysis, buffer exchange, and protein quantitation

Cells were mixed with lysis buffer containing 7 M urea, 2 M thiourea, 100 mM DTT, 2% *n*-octyl G-D-glucopyranoside (OG), 10% glycerol, 10 mM sodium orthovanadate, 10 mM sodium fluoride (all from Sigma, St. Louis, MO), 0.5% Biolyte ampholyte (BioRad, Hercules, CA), and protease inhibitor cocktail (Roche Diagnostics, Mannheim, Germany) with vortexing at room temperature for 1 h. Cellular debris and other insoluble materials were removed by centrifuging the mixture at $80\,000 \times g$ for 1 h 15 min. The supernatant was subjected to buffer exchange in order to replace the lysis buffer with start buffer (SB) (composition described later) for chromatofocusing (CF) using a PD-10 G-25 column (Amersham Biosciences, Piscataway, NJ). The protein concentration was determined using the Bradford Protein Assay kit with BSA (BioRad) standard.

2.1.3 Chromatofocusing (CF)

The CF experiment was performed using a Beckman System Gold model 127 pump and 166 UV detector module (Beckman-Coulter, Fullerton, CA) with an HPCF-1D prep column (250 mm length × 4.6 mm id, Eprogen, Darien, IL). A linear pH gradient was generated using a combination of SB composed of 6 M urea, 25 mM Bis-Tris, and 0.2% OG and elution buffer (EB) containing 6 M urea, 0.2% OG, and 10% polybuffer 74 (Amersham Biosciences). Saturated iminodiacetic acid (Sigma) was used to adjust the pH of SB at 7.2 and EB at 3.9. The column was first equilibrated in SB until the pH of the column was the same as SB by monitoring with a post-detector online assembly of a pH-flow cell (Lazar Research Laboratories, Los Angeles, CA). After equilibration, ~10 mg of sample was loaded onto the column at a low flow rate to allow for interactions of the proteins with the binding sites. Once a baseline was achieved, solvent flow was switched to EB and the flow rate was set to 1 mL/min for CF fraction collection at the intervals of 0.2 pH units along the linear gradient, where the elution profile was recorded at 280 nm. At the end of the gradient, the column was flushed with 1 M sodium chloride (Sigma) to remove any proteins still bound to the column. All collected samples were stored at −80°C until further analysis.

2.1.4 Nonporous silica RP-HPLC

Each CF fraction was loaded onto a nonporous silica RP (NPS-RP) HPLC column for further separation. An ODSIII-E (8×33 mm^2) column (Eprogen) packed with 1.5 μm NPS was used to achieve high separation efficiency. The separation was performed at a flow rate of 1 mL/min using a water/ACN solvent system (A was 0.1% TFA in deionized water and B was ACN and 0.1% TFA) and the gradient used was: 5–15% B in 1 min, 15–25% B in 2 min, 25–31% B in 3 min, 31–41% B in 10 min, 41–47% B in 3 min, 47–67% B in 4 min, 67–100% B in 1 min, followed by maintaining the system at 100% B for 3 min. Separation was monitored at 214 nm using a Beckman 166 model UV detector (Beckman-Coulter). Purified protein peaks were collected in deep-well 96-well plates using an automated fraction collector (model SC 100; Beckman-Coulter), controlled by in-house-designed DOS-based software. The column was maintained at 60°C during separation to enhance reproducibility, speed, and resolution. Following protein fractionation, the samples were stored at −80°C until further use.

2.2 Protein microarrays

2.2.1 Array spotting

All fractions were transferred to shallow-well print plates (BioRad) and were lyophilized to dryness. The samples were resuspended in printing buffer, consisting of 62.5 mM Tris-HCl (pH 6.8), 1% w/v SDS, 5% w/v DTT, and 1% glycerol in 1 × PBS, and were left agitating on an orbital shaker overnight. Printing was accomplished by depositing five droplets of ~500 pL each per fraction using a piezoelectric dispenser (Nanoplotter 2, GeSiM). Superamine glass slides (TeleChem International) were utilized for printing. Distance between spots was maintained at 600 μm and spot sizes were found to be ~450 μm. Prior to processing all slides were kept sealed in a dessicator.

2.2.2 Array processing with Pro-Q diamond dye

Glass slides were blocked overnight in 1% BSA (Roche) in 1 × PBS-T (0.1% Tween 20). They were then incubated for 1 h in Pro-Q Diamond phosphoprotein gel stain (Invitro-

gen). The slides were then washed in destaining solution (Invitrogen) three times for 10 min each, then rinsed with nuclease free water, and dried by centrifugation. The slides were scanned in the green channel using an Axon 4000A scanner, and GenePix Pro 6.0 software (Molecular Devices, Sunnyvale, CA) was used for data acquisition and analysis. Spots were considered to be positively fluorescent if background subtracted intensity of the spot was $\geq$X2 the local background intensity around the spot.

2.2.3 Array processing with antityrosine antibodies

Glass slides processed and scanned with Pro-Q diamond dye were rehydrated and then incubated in mouse monoclonal antiphosphotyrosine, 4G10 clone antibody (Upstate, Charlottesville, VA) diluted to 2 μg/mL in probe buffer (5 mM magnesium chloride, 0.5 mM DTT, 0.05% Triton X-100, and 5% glycerol in 1 × PBS). After primary incubation the slides were washed (five times, 5 min each) in probe buffer. Secondary incubation was performed for 1 h using donkey anti-mouse antibody conjugated to fluorescent cy5 at a concentration of 1 μg/mL in probe buffer. The slides were finally washed (five times, 5 min each) in probe buffer and scanned in the red channel. Once again, spots were considered to be positively fluorescent if background subtracted intensity of the spot was $\geq$X2 the local background intensity around the spot.

2.3 Removal of SDS from samples

Prior to digestion and protein identification by MS samples were cleaned using Detergent-OUT SDS-300 spin columns (G-Biosciences, St. Louis, MO) to remove residual SDS that was present during reconstitution into print buffer as per the user guide. In short, spin columns were inverted to re-suspend resin and liquid was drained off by spinning at 1000 × *g* for 10 s. Columns were then equilibrated with 1.5 mL deionized water which was collected in a centrifuge tube and discarded. Sample was then applied to the spin columns and was let to stand for 5 min. After the columns were loaded they were centrifuged at 1000 × *g* for 30 s and the SDS-free sample was collected in a centrifuge tube.

2.4 Trypsin digestion

The samples were dried down to 10 μL, and then 40 μL of 100 mM ammonium bicarbonate and 10 μL of 10 mM DTT were added to sample. The samples were incubated at 60°C for 20 min to allow for reduction of disulfide bonds. 0.5 μL of TPCK modified sequence grade trypsin (Promega) was added and the samples were incubated at 37°C overnight. Digestion was stopped by adding 1 μL of TFA to the digestion mixture.

2.5 Peptide sequencing by LC-MS/MS

Digested samples were separated by a capillary RP column (MagicAQ C18, $0.1 \times 150\ mm^2$) (Michrom Biosciences, Auburn, CA) on a Paradigm MG4 micropump (Michrom Biosciences) with a flow rate of 300 nL/min. The gradient was started at 3% ACN, ramped to 35% ACN in 25 min, 60% ACN in 15 min, 90% in 1 min, maintained at 90% ACN for 1 min, and finally ramped back down to 3% in another 1 min. Both solvents A (water) and B (ACN) contained 0.1% formic acid. The resolved peptides were analyzed on an LTQ mass spectrometer (Thermo, San Jose, CA) with a nano-ESI platform (Michrom Biosciences). The capillary temperature was set at 200°C, the spray voltage was 2.5 kV, and the capillary voltage was 20 V. The normalized collision energy was set at 35% for MS/MS. The top five peaks were selected for CID. Precursor selection was based upon a normalized threshold of 30 counts/s. MS/MS spectra were searched using the SEQUEST algorithm incorporated in Bioworks software (Thermo) against the Swiss-Prot human protein database with trypsin as the enzyme. Additional search parameters were as follows: (i) allowing two missed cleavages; (ii) possible modifications, oxidation of M and phosphorylation of S, T, and Y; (iii) peptide ion mass tolerance 1.50 Da; (iv) fragment ion mass tolerance 0.0 Da; (v) peptide charges +1, +2, and +3. The filter function in Bioworks browser was applied to set a single threshold to consider peptides assigned with X_{corr} values as follows: $\geq$1.5 for singly charged ions, $\geq$2.5 for doubly charged ions, and $\geq$3.5 for triply charged ions.

3 Results and discussion

The overall strategy we used for the large-scale analysis of cellular protein phosphorylation status is outlined in Fig. 1. Fractionation of the sample to reduce complexity, was achieved by separation in two dimensions, initially by CF (according to the protein p*I*), and then by RP-HPLC, according to their hydrophobicity. Fractions were carefully collected by peaks and each cell line resulted in approximately 1200 fractions after the complete 2-D separation. The fractionated proteins were then printed onto microarrays and analyzed by hybridization with a universal phosphoprotein stain, and with antibodies specific to phosphorylated tyrosine residues. Hundred forty spots were found to exhibit a positive response to the Pro-Q dye. Antiphosphotyrosine antibodies did not give any additional information compared to the Pro-Q Diamond dye suggesting that sensitivities of both forms of detection were comparable. It is therefore possible to solely use the Pro-Q Diamond dye for detection purposes, hence saving on the high antibody-based detection costs. However anti-phosphotyrosine antibodies would be preferred in cases where only signaling cascades controlled by tyrosine phosphorylation are being sought. Sequence analysis of specific phosphoproteins for confident identification was achieved by

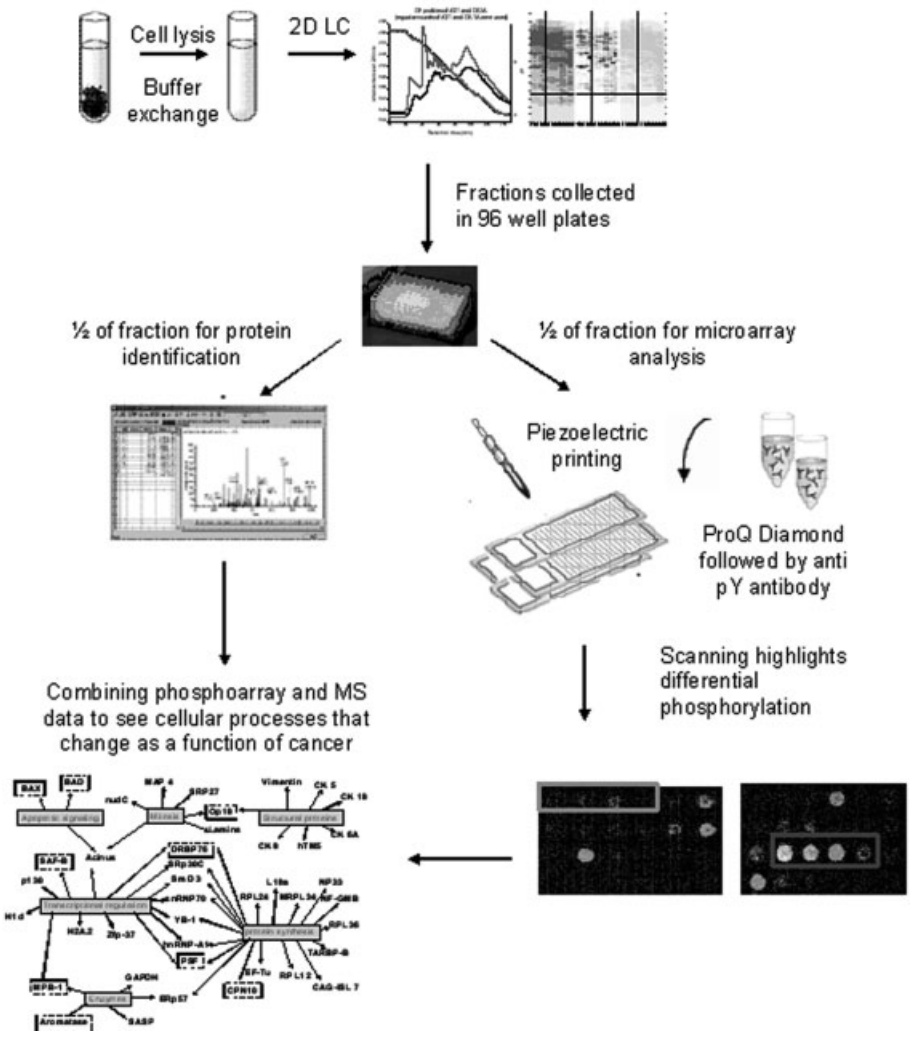

Figure 1. Microarray strategy for global evaluation of phosphorylation changes as a function of disease.

peptide sequencing using MS/MS. This combinatorial approach overcomes many of the limitations inherent in single-method analyses. Phosphorylation sites have proved difficult to identify by MS alone due to poor ionization efficiency and low abundance of phosphopeptides. Additionally, mass spectrometric methods are not reliable for assessing phosphorylation in a time-efficient manner. The proposed strategy is high-throughput in nature and a method of choice in initial screening to find differentially expressed proteins over the whole proteome in a sample of interest.

3.1 2-D liquid separation and microarray reproducibility

A comparison of the 2-D liquid separation (pH 4.0–7.2) is illustrated in Fig. 2. On the left is a 2-D UV map of the pre-malignant AT1 cell line, while on the right is the same for the malignant CA1a cell line. In the center is the comparison of the two maps. It can be seen that while the overall 2-D maps are very similar for both cell lines, several differences are revealed. In particular, many proteins are highly expressed in the malignant cell line, CA1a in the pH range 6.6–7.0 (corresponding to lanes 13 and 14 in Fig. 2). Most of these proteins elute during the first half of the HPLC run. Sixty-nine proteins were detected in the pH range 6.6–7.0 based upon LC-MS/MS experiments in the malignant CA1a cell line.

Comparative screening of the protein microarrays was achieved using the global phosphoprotein stain Pro-Q Diamond and antibodies specific to phosphorylated tyrosine residues. To investigate the binding properties of Pro-Q phospho-stain and antibodies, protein, and peptide standards were printed on SuperAmine slides. The slides were then probed initially with the phosphoprotein stain, Pro-Q Diamond, followed by a monoclonal anti-phosphotyrosine antibody (Fig. 3a). While ovalbumin and β-casein solely contain phosphoserine and phosphothreonine residues and therefore fluoresce green as a result of staining, the phosphotyrosine peptide (pY) mixture appears red. This occurs because the antibody for phosphotyrosine displaces the Pro-Q and binds to the phosphotyrosine residues present in that

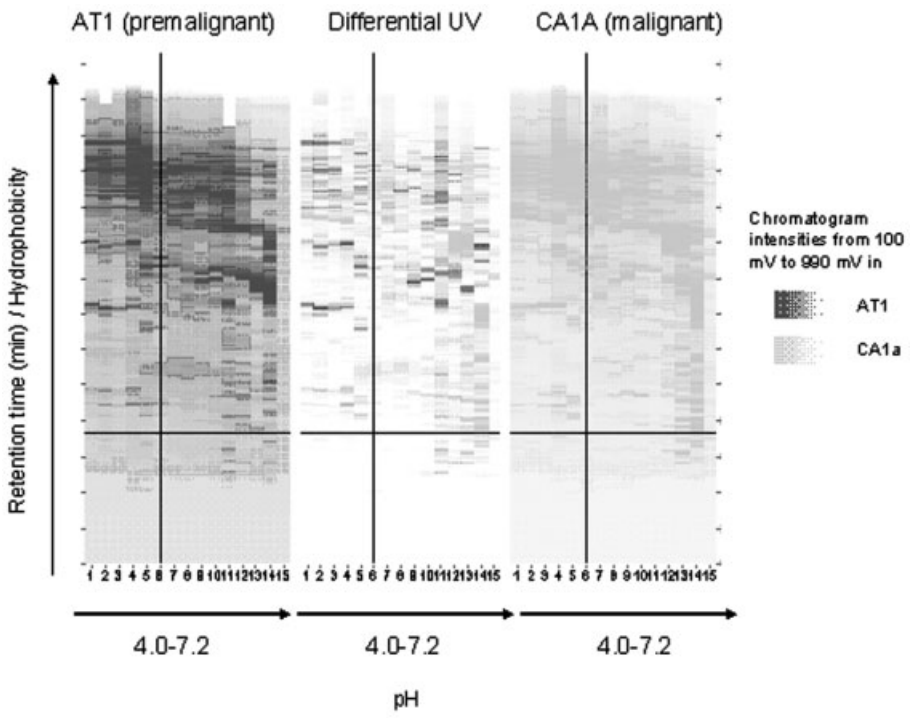

Figure 2. 2-D liquid separation of premalignant AT1 and malignant CA1a cell lines. Each lane represents a pH fraction different by 0.2 units. Vertical axis refers to the retention time during the separation. Intensity of the bands correspond to peak heights which ranged from a value of 100–990 mV. Difference between premalignant and malignant sample appears in the middle panel.

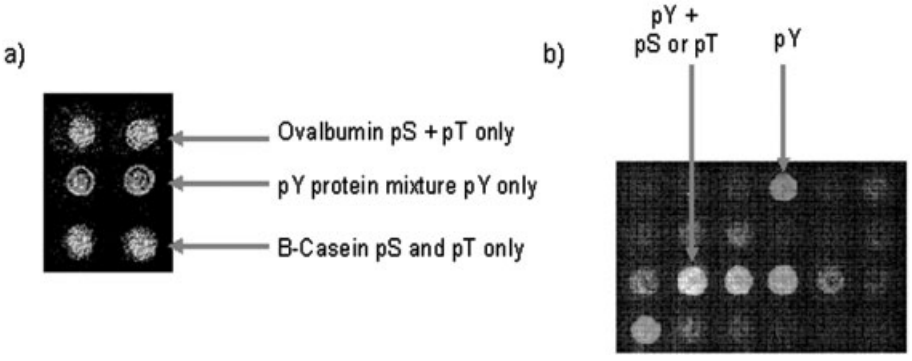

Figure 3. Detecting phosphoproteins on microarrays using Pro-Q Diamond dye and antiphosphotyrosine antibodies. (a) A study done with standards where ovalbumin, B-casein, and a mixture of tyrosine phosphorylated proteins were used. The figure is shown in gray scale but when probed with both Pro-Q and anti-pY antibody, the fluorescent labels are such that solely pY proteins appear red, a mixture of pY and pS or pT appear yellow and solely pS or pT appear green. (b) An image of a section of a protein microarray-containing fractionated proteins from a malignant breast whole cell lysate.

spot. Subsequently, a red fluorescently tagged secondary antibody (in this case, an anti–anti-phosphotyrosine antibody conjugated to cy5) binds to the primary anti-phosphotyrosine antibody resulting in a red spot. A section of microarray generated by spotting of premalignant AT1 and malignant CA1a is also shown in Fig. 3b. It can be seen that several fluorescing protein spots indicate the presence of phosphorylation. More importantly, Fig. 3b shows that the protein contents that were being used in the 2-D separation were sufficient for microarray analysis.

Given the dynamic nature of cellular phosphorylation, we undertook a reproducibility study in order to better indicate the biological relevance of our phospho-profile findings. Three separately grown CA1a cell line batches and two separately grown AT1 cell line batches were independently subjected to the entire analytical strategy, including 2-D liquid separations, protein microarray, and MS. Several pH ranges were selected to assess reproducibility for all samples.

Figure 4 illustrates the results obtained. When looking at the CF result (Fig. 4a), where pH fractions as collected could be monitored online for pH *via* a pH electrode assembly, it can be seen that for all separations a reproducible pH gradient was obtained. Furthermore, it can be seen for the CA1a cell line that all separated samples resulted in very similar

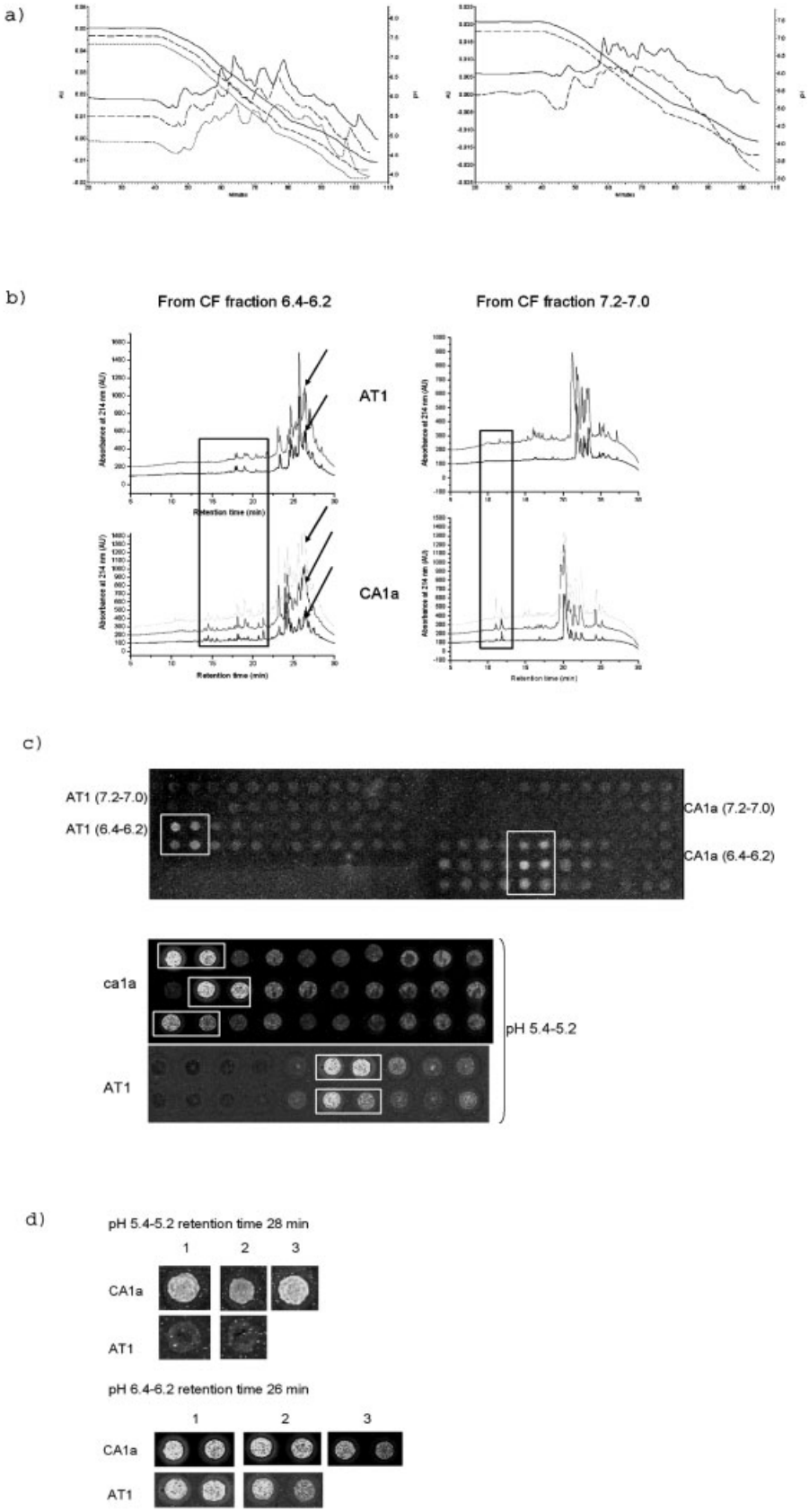

Figure 4. Comprehensive study to assess reproducibility of the method. (a) CF chromatograms of three ca1a separations are shown on the left and of two AT1 separations are shown on the right. In all cases 4.5 mg of sample was loaded (one AT1 separation was performed with only 3 mg of total protein). Co-plotted with the chromatograms are pH profiles to illustrate that the pH gradient was consistent in all separations. (b) Second dimension chromatograms of all batches of cell lines for pH ranges 6.4–6.2 and 7.2–7.0. Arrows along the chromatogram illustrate peaks that are shown in subsequent microarray data. (c) Array images of samples from pH fractions 7.2–7.0, 6.4–6.2, and 5.4–5.2 to illustrate reproducibility throughout the separation space. (d) Sections of microarray data showing an example of reproducible positive spots that are unique to ca1a (pH 5.4–5.2, retention time 28 min) and that are found in all cell lines (pH 6.4–6.2, retention time 26 min). Peaks corresponding to the positive spots found in all cell lines are indicated by arrows in Fig. 4b.

and reproducible separation profiles. Similar separation profiles were also observed for the two batches of AT1 cell lines run. However, although the peak patterns were very similar they were not identical as in the case of CA1a. This difference was explained by the fact that while all other samples were loaded at a total protein content of 4.5 mg, one of the AT1 samples had a lower total protein content of only 3 mg which resulted in an overall lower signal during the acquisition of the chromatogram. A comparison of the two batches of chromatograms suggests some subtle differences between CA1a and AT1 particularly in the higher pH range of about 7.0–6.2 and in the lower pH range around 5.6–5.2.

In order to further assess these subtle differences, selected pH ranges were subjected to NPS-RP-HPLC. Example chromatograms illustrating these separations are shown in Fig. 4b. A high level of reproducibility is seen in both the independently grown batches of CA1a and AT1 samples analyzed. Furthermore, the subtle differences that were seen in the CF profiles are better visualized in the second dimension. It can be seen that the malignant CA1a cells contains more hydrophilic protein peaks relative to the premalignant AT1 cells.

Fractionated samples from the second dimension were arrayed on glass slides and probed with Pro-Q diamond dye to assess the phosphorylation status of the proteins. It is possible that while the chromatograms appear reproducible, the phosphorylation status of the protein may not be the same, making it necessary to assess reproducibility at the microarray level. Five slides were printed and probed with Pro-Q dye to assess the reproducibility of the printing and hybridization process. Figure 4c shows slide images of spots that were arrayed from selected pH ranges. It can be seen that all spots show consistently similar size and shape indicating that the printing process is consistent and reproducible. Slight variation in background intensities between the slides can be attributed to variation in slide surfaces and experimental variation during hybridization. However, these variations do not alter the number of positive spots of the array and therefore do not affect the results significantly. Figure 4d illustrates sample biological reproducibility data obtained using the three CA1a and the two AT1 batches. It can be seen that for the pH range 6.4–6.2 there is a phosphorylated protein that elutes around retention time 26 min for all samples of CA1a and AT1 that were analyzed. However, for the pH range 5.2–5.0 there is a phosphoprotein (retention time 28 min) that is present only in CA1a samples. The reproducibility experiment revealed that consistent, differential phosphoprotein expressions were achievable across samples and batches.

It was also important to verify that the proteins present in consistently detected spots on the microarray were in fact the same proteins across samples. To this end, SDS was removed from selected sample fractions to be printed on arrays (as outlined in Section 2), proteins were trypsinized and then analyzed by MS/MS. Table 1 shows the protein IDs of the two spots that appeared positive for the CA1a samples in the pH range 6.4–6.2. In all cases, the proteins present in specific microarray spots were the same proteins. These analyses show that the strategy and the techniques are highly reproducible and confirm that the differential expression of specific phosphoproteins is maintained in the MCF10A tumor progression model.

3.2 Cell-associated phosphoprotein profiles

All spots representing the same region of the 2-D UV map from the two cell lines were compared to identify differential phosphorylation profiles. Premalignant and malignant samples were printed on microscopic glass slides with a chemically modified amine surface for studies with Pro-Q and antiphosphotyrosine antibodies. For each comparison, at least five replicate slides were processed. Of the phosphoproteins whose modification sites were identified, 11 proteins were seen to be phosphorylated in the premalignant cell line but not the malignant cell line, and 16 proteins were seen to be phosphorylated in the malignant cell line but not the premalignant cell line. Examples of the differences observed, together with the identity of the protein as deter-

Table 1. Protein IDs and peptides identified for selected microarray spots depicted in Fig. 4c

Sample	Protein ID	Score	Peptides sequences	Coverage
Ca1a_spot1	Lamin-A/C	400	15	25
Ca1a_spot2	Lamin-A/C	410	19	33
	Protein disulfide-isomerase A3 precursor	370	15	31
Ca1a_spot1	Lamin-A/C	450	20	33
Ca1a_spot2	Protein disulfide-isomerase A3 precursor	380	15	29
	Lamin-A/C	340	17	30
Ca1a_spot1	Lamin-A/C	410	18	33
Ca1a_spot2	Lamin-A/C	480	20	34
	Protein disulfide-isomerase A3 precursor	360	14	30
AT1_spot1	Lamin-A/C	410	19	32
AT1_spot2	Protein disulfide-isomerase A3 precursor	240	11	21
	Lamin-A/C	180	8	14

mined by MS/MS, are illustrated in Fig. 5. In some cases a protein eluted over multiple peaks due to diffusional broadening during sample collection. These proteins appear in multiple spots in the figures. Furthermore, there were instances where more than one phosphoprotein eluted at almost the same retention time. In these cases both protein identities are shown in the figure. Overall, 51 phosphorylation sites from a total of 27 proteins were identified over a pH range of 7–4. In addition, 47 previously reported phosphoproteins were also identified, but no phosphorylation site verification was obtained through the MS/MS data. Although dynamic exclusion was used to ensure that peptides eluting over a longer time were not continuously selected for MS/MS analysis, it is possible that more sites were not identified due to the low signal intensities of phosphopeptides which rendered them undetectable using the top five ion peak selection used during our MS/MS runs. Furthermore, three phosphoproteins were shown to not be differentially expressed in the two cell lines. All phosphoproteins identified with site verification are listed in Table 2, along with information about the number of peptides and protein coverage pertinent to protein identification. Table 1 of Supporting Information also lists all phosphoproteins identified without site verification. Site verification was not possible for these peptides due to low sample amounts. We did investigate phosphopeptide enrichment using titanium dioxide tips to improve yield, but without improvement. The results presented herein correlate well with previous work where approximately 155 spots in a 2-D gel stained positive for phosphorylation using the Pro-Q Diamond dye [34]. In another study about 100 proteins showed a change in phosphorylation upon stimulation of fibroblast cells where detection on 2-D gels was facilitated by using antiphosphotyrosine and antiphosphoserine antibodies [35]. Our proposed strategy bypasses problems associated with 2-DE while providing equivalent and complementary information about protein phosphorylation at the intact protein level. This can be especially useful when site verification from mass spectrometric data is difficult due to poor phosphopeptide spectra, which is often the case.

The pie chart in Fig. 6 shows the cellular distribution of proteins whose modification sites were verified regardless of whether the phosphorylation was found in the premalignant or malignant cell line. Interestingly, out of the 27 differentially phosphorylated proteins whose modified sites could be verified by MS/MS, 18 were nuclear proteins. This trend of differential phosphoprotein expression in the nuclear region was also observed for those proteins whose sites were not verified. Closer examination of the proteins showed that the malignant CA1a cell line exhibited increased phosphorylation of nuclear proteins compared to the premalignant AT1 cell line.

It should be noted that a majority of the proteins that were detected and identified as being differentially phosphorylated in this work are of high to medium abundance. In this work, we observed 85 differentially expressed spots (corresponding to a total of 75 phosphoproteins of which we

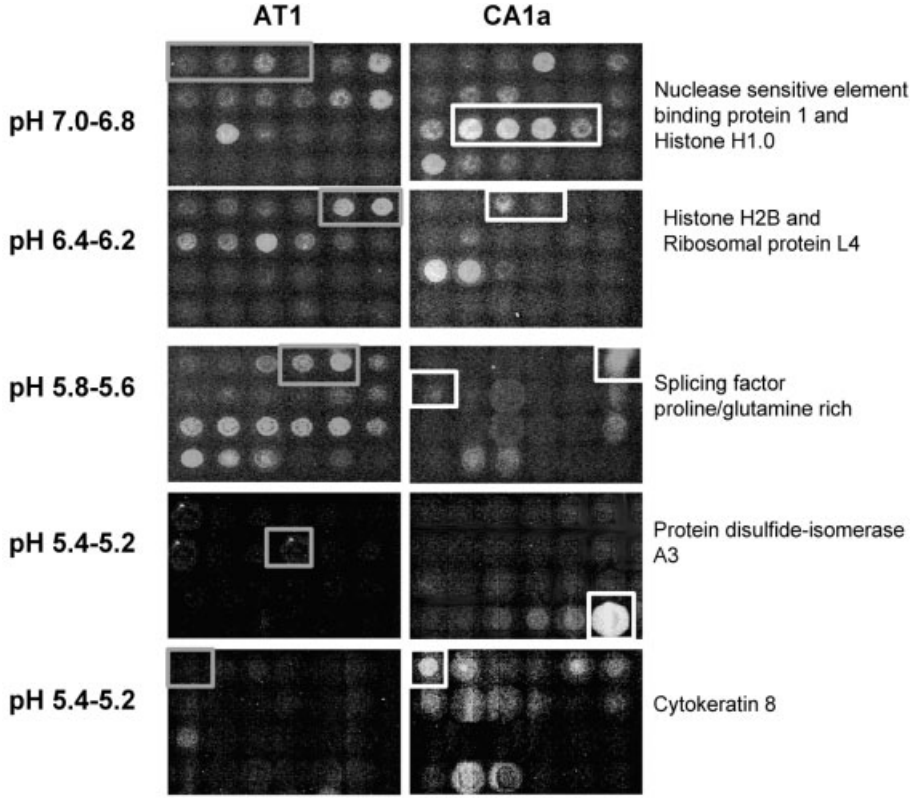

Figure 5. Selected microarray images showing comparison of spots where differential phosphorylation was observed between premalignant and malignant breast cell lines over different pH regions. Protein IDs as determined by MS/MS are shown beside the image. For some proteins, multiple consecutive spots light up due to diffusional broadening during peak collection. In some cases more than one phosphoprotein was identified in the same collected fraction. In such cases, both phosphoproteins are listed.

Table 2. Phosphoproteins identified with confirmation of phosphorylation sites. Additional information was obtained from the Swiss-Prot database

Accession no. phosphoprotein	pH range	Pep. identified	% Coverage	Peptide + site	Previously reported site	AT1	CA1A	Cellular location
P50914 60S ribosomal protein L14	7.0–6.8	4	18	S138 (AALLKApSPK)	none		X	Nucleus
Q14978 Nucleolar phosphoprotein p130	7.0–6.8	2	3	S303 (pSLGTQPPK)	pT607, pT610, pS623, pS643, pS698		X	Nucleus
P83731 60S ribosomal protein L24	7.0–6.8	2	13	T24 (pTDGKVFQFLNAK)	pT83, pS86		X	
Q9BQ48 39S ribosomal protein L34	7.0–6.8	3	26	S89 (pSLSH)			X	Mitochondria
Q9Y3U8 60S ribosomal protein L36	7.0–6.8	4	27	T17 (VpTKNVSK)			X	
P62318 Small nuclear ribonucleoprotein Sm D3	7.0–6.8	1	7	S93 (NQGpSGAGRGK)			X	Nucleus
Q13428 Treacle protein	7.0–6.8	4	4	S959, S964 (IAP-KApSMAGApSSSK)	pT173, pS890, pS1034, pS1151, pS1299, pS1301, pS1394		X	Nucleus
Q9Y6Q3 Zinc finger protein 37 homolog	6.8–6.6	2	4	T234 (QDKIQpTGEKHEK)	none		X	Nucleus
P02545 lamin A/C	5.4–5.2	39	55	S17, S18 (SGA-QApSpSTPLSPTR), S390, T394 (LRLpSPSPpTSQR)	S22, S390, S392, S652. By similarity S407, S496, T505, S507, T510,		X	Nucleus
Q09666 neuroblast differentiation associated protein AHNAK	5.2–4.8	2	4	T2727 (VpTFPKMKIPK)	S264, S312	X		Nucleus
P07355 annexin A2	5.2–5.0	3	7	S84 (ELApSALK)	S18, Y24, S26	X		Plasma membrane
P11511 Cytochrome P450 19A1	5.2–5.0	1	2	T391 (KGpTNIILNIGR)	none	X		Membrane
Q14562 ATP-dependent helicase DHX8	5.2–5.0	2	5	T914, T915 (DEMLpTp-TNVPEIQR)	none		X	Nucleus
Q02539 histone H1.1.	5.2–5.0	2	6	T151 (KSVKpTPK), T203 (pTAKPK)	none	X		Nucleus
Q03252 lamin B2.	5.2–5.0	13	20	S402, S401, S400 (ATSpSpSpSGSLSATGR)	similarity S427	X		Nucleus
P02545 lamin A/C	5.2–5.0	36	56	S390, S392, T394 (LRLpSPpSPpTSQR) S403, S404, S406, S407 (ApSpSHpSpSQ TQGGGSVTK)	S22, S390, S392, S652. By similarity S407, S496, T505, S507, T510,	X		Nucleus
P02545 lamin A/C	5.2–5.0	32	48	S390, S390, T394, (LRLpSPpSPpTSQR)	S22, S390, S392, S652. By similarity S407, S496, T505, S507, T510,		X	Nucleus
P84103 Sslicing factor, arginine/serine-rich 3	5.2–4.8	6	32	S108 (RRpSPPPR), S126, S128, S130 (pSRpSLpSR)	Extensively phosphorylated on serine residues in the RS domain	X		Nucleus
Q09666 neuroblast differentiation associated protein AHNAK	5.0–4.8	11	9	T2727 (VpTFPKMKIPK)	experimental S264, S312		X	Nucleus
Q07812 apoptosis regulator BAX, membrane isoform α	5.0–4.8	2	6	T135, T140 (pTIMGWpTLDFLR)	none	X		Membrane
P16403 histone H1.2	5.0–4.8	3	18	S112 (KAApSGEAK)	similarity S36		X	Nucleus
P08779 cytokeratin 16	5.0–4.6	3	8	Y249 (EELApYLR)	none	X		Cytoskeleton
P05787 Cytokeratin 8	5.0–4.8	20	41	S43 (VGSpSNFR)	S24, S74, S432, S451. By Similarity S9, S13, S22, T26, S27, S34, S37, S43, S417, S424, S475, S478	X		Cytoskeleton
Q15424 scaffold attachment factor B	5.0–4.8	2	1	S383, S384, S389 (MpSpSPEDDpSDTK)	by similarity S344	X		Nucleus

Table 2. Continued

Accession no. phosphoprotein	pH range	Pep. identified	% Coverage	Peptide + site	Previously reported site	AT1	CA1A	Cellular location
P28001 histone H2A.a	4.8–4.6	3	27	T120 (pTESHHK)	S2, T121		X	Nucleus
O14929 histone acetyl-transferase type B catalytic subunit	4.8–4.6	2	5	S350, Y351 (pSpYRLDIKR)	none	X		Nuclear in S Phase otherwise cytoplasmic
P08621 U1 small nuclear ribonucleoprotein 70 kDa	4.8–4.6	12	26	S226 (YDERPGPpSPLPHR)	S226		X	Nucleus
P08670 vimentin.	4.8–4.6	25	56	S54, S55 (SLYApSpSPGG-VYATR), S28, Y29 (pSpYVTTSTR)	S5, S7, S8, S9, S10, S39, S42, S56, S72, S73, Y117, S420, S430, T458, S459. By similarity S25, S26, S34, S47, S51, S66, S83		X	
Q9UKV3 apoptotic chromatin condensation inducer in the nucleus	4.6–4.4	8	6	S1004 (TAQVPpSPPR)	S240, S243, S365, S386, S388, S657, S661, S676, S1004, T414, T682. By similarity S384		X	Nucleus
P20700 lamin B1.	4.2–4.0	12	23	S395 (LSPSPSpSRVTVS-RASSSR)	T20, S23, S391		X	Nucleus
P02545 lamin A/C	4.2–4.0	32	47	S17, S18 (SGA-QApSpSTPLSPTR), S94 (KTLDpSVAK), S390, S392, T394 (LRLpSPpSPpTSQR)	S22, S390, S392, S652. By similarity S407, S496, T505, S507, T510,		X	Nucleus

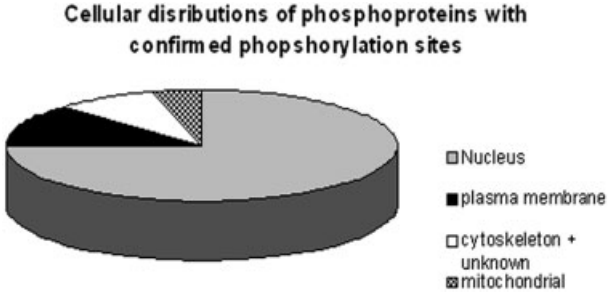

Figure 6. Pie chart illustrating subcellular location of phosphoproteins whose phosphorylation sites were confirmed by MS in both the AT1 and CA1a cell line combined. Closer examination showed a majority of these phosphoproteins to be present in the CA1a cell line (see Table 1).

were able to identify phosphorylation sites from 27 proteins) although we observed a total of 140 protein spots that responded to Pro-Q Diamond dye. The information that can be found from this work can therefore shed light on the downstream effects of phosphorylation signaling cascades. However, information about the very first changes that occur in a pathway were not detected since these occur on molecules with very low copy numbers in the cell which are generally below the detection limit of the Pro-Q dye.

An interesting phenomenon that we observed in our experiments was the shifts in p*I* due to phosphorylation. For example, in Table 1 it can be seen the protein lamin A/C appears multiple times. This protein was seen over more than one pH range. In addition it was found that the phosphorylation sites on the protein that were detectable using the unenriched samples were different for each pH range where the protein was observed. This phenomenon illustrates an important aspect about the effect of PTMs on protein p*I*. Previous work from our laboratory has shown that addition of a PTM on a protein changes the protein p*I* [36] and microarray data from this study further support these findings.

3.3 Functional grouping of phenotype-associated phosphoprotein profiles

Many of the differentially expressed phosphoproteins identified in this study fall under distinct categories with respect to the biological processes in which they are involved. Figure 7 summarizes these proteins according to their functional role in cellular processes. The majority of differentially phosphorylated proteins were found to be upregulated in the malignant CA1a cell line. A few key proteins that were found to be more phosphorylated in the nonmalignant AT1 appear in a box with broken lines in the same figure. Transcriptional and translational proteins were in the majority, while mitotic and apoptosis-related proteins were also represented. In addition, a separate class of enzymes as well as proteins that maintain cytoskeletal integrity were observed to change their phosphorylation state as a function of malignant cellular phenotype. A discussion of some of the known roles of the phosphoproteins identified in this study is given below.

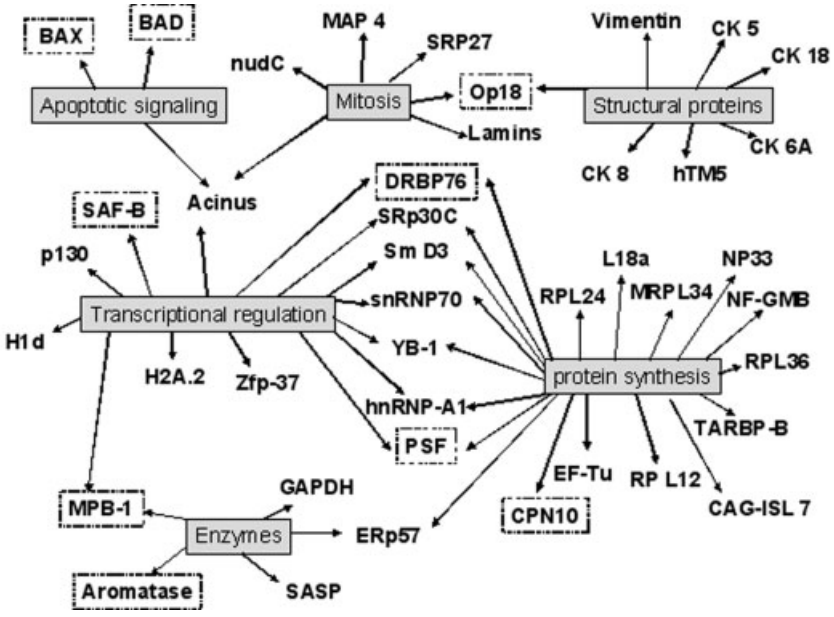

Figure 7. Functional classification of proteins differentially phosphorylated in the premalignant and malignant breast cell lines. Majority of phosphoproteins were found in the malignant, CA1a. In cases where a phosphoprotein was found in AT1 and not CA1a, it appears in a box with broken lines.

3.3.1 Apoptotic signaling

Proteins involved in the regulation of apoptosis are important determinants of cell proliferation and survival in malignant phenotypes. Stimulatory growth factor signaling and inhibitory stress factors initiate signal transduction pathways that regulate apoptosis *via* altering the phosphorylation of key regulating proteins. Three proteins important in the regulation of apoptosis, Bad, Bax, and Acinus were differentially phosphorylated in AT1 and CA1a cells. While phosphorylated acinus was only found in CA1a, Bad, and Bax phosphorylated forms were uniquely seen in AT1.

Growth factor induced phosphorylation of BAD protects cells from apoptotic stimuli. PI3K/Akt, Ras/MAPK/Rak, and PKA pathways all phosphorylate BAD. When serines at 112, 136, and 155 are phosphorylated, BAD is bound to an inactive complex [37] In LNCaP human prostate cancer cells, phosphorylated sites necessary for activity varied with the survival signaling pathway [38]. Because malignant cells would be expected to have diminished sensitivity to apoptotic signals, phosphorylation of BAD in AT1 relative to CA1a suggests that additional sites other than the previously reported critical three serines are phosphorylated in AT1 cells.

The consequence of phosphorylated threonines at 135 and 140 in Bax in AT1 cells is unknown. Both apoptotic and anti-apoptotic activities have been associated with phosphorylation at different sites in other cells. Phosphorylation of Ser-184 inhibits proapoptotic function of Bax in A549 human lung cancer cells [39] whereas phosphorylation of Thr-167 in Bax activates apoptotic activity in HepG2 human hepatoma cells [40].

Acinus, apoptotic chromatin condensation inducer in the nucleus protein (Accession number Q9UKV3), is also a direct target of Akt and phosphorylation on Ser-422 and Ser-573 inhibits apoptosis in HEK293 cells, possibly by preventing caspase-mediated cleavage to a form that is necessary for chromatin condensation and apoptosis [41]. Acinus was uniquely seen to be phosphorylated in only the malignant CA1a cells, according to both the microarray and MS data. The phosphorylation site that was identified was located on S1004, as shown in Fig. 8a. Multiple peptides from the protein were sequenced, some of which were in the aa 800–900 region of the protein. Interestingly it is known that the active form of the protein is a caspase-cleaved isoform, p17 which consists of the sequence aa 987–1093. It was thus confirmed that the unprocessed, and therefore inactive, isoform was present in the cell line suggesting the absence of apoptotic chromatin condensation. Suppression of apoptosis may be instrumental to the malignant nature of the cell line.

3.3.2 Transcriptional regulation

This study showed that several proteins involved in transcriptional regulation were differentially phosphorylated in the two cell lines. Several histones were more phosphorylated in CA1a. Histones are typically positively charged to hold the negatively charged DNA in its condensed form. Phosphorylation of histones imparts negative charge so that DNA is less tightly bound and is thus available for manipulation. Zfp-36 and nucleolar phosphoprotein p130 are transcriptional regulatory proteins that were seen to be more phosphorylated in the malignant CA1a. SAF-B is a scaffold attachment factor that regulates the formation of the transcriptosomal complex and is also thought to be a corepressor of the ER, a pivotal factor in breast cancer phenotypes. SAF-B is known to decrease cell proliferation by reducing transcription of HSP-27. Interestingly this protein was phosphorylated in the premalignant AT1.

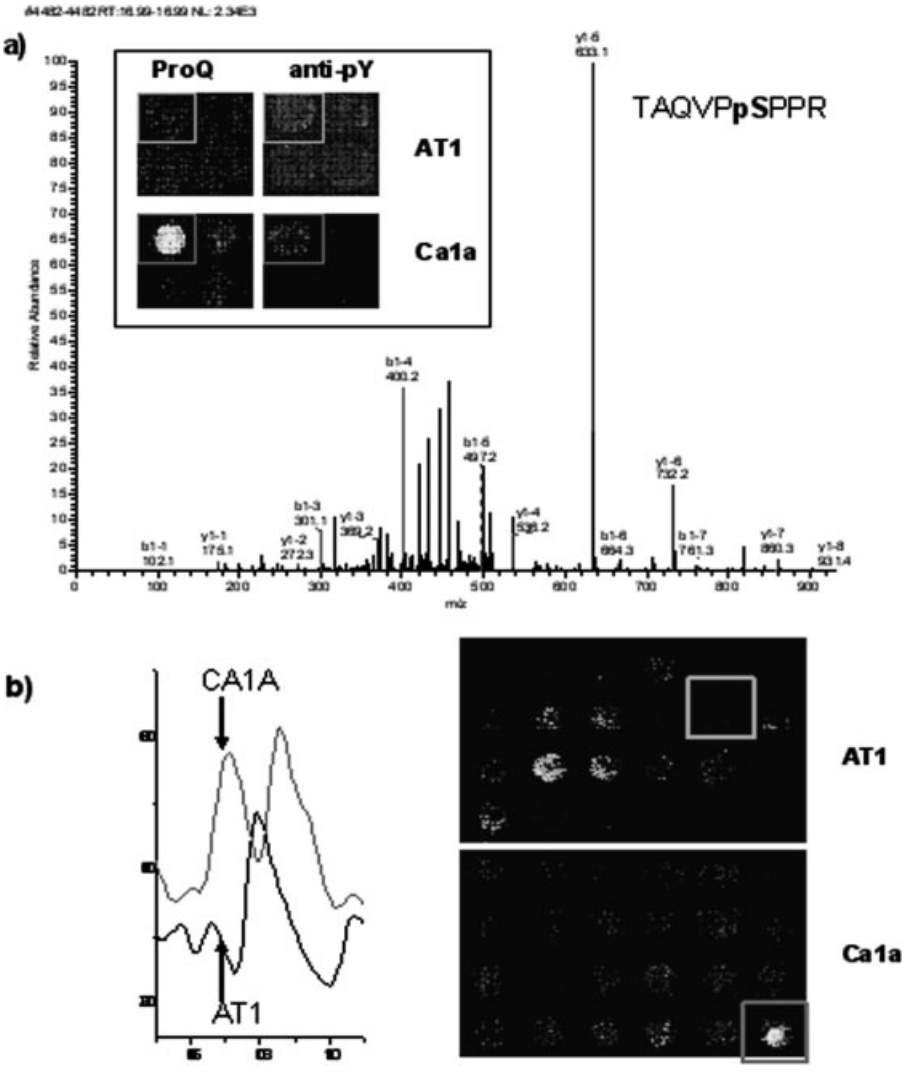

Figure 8. (a) Tandem mass spectrum (with +1 ion series highlighted) of selected phosphopeptide from apoptotic condensation inducing factor with inset showing phosphorylation difference between AT1 and CA1a as seen on the microarray. (b) Microarray image together with complementary portion of RP chromatogram where 60S ribosomal protein L14 was found to be phosphorylated in only CA1a.

3.3.3 Protein synthesis

In addition to an increase in transcription-related phosphorylation, a parallel increase was seen in translational proteins in the malignant CA1a cell line compared to the pre-malignant AT1. Protein identifications as confirmed by MS/MS showed the expression of larger numbers of ribosomal proteins in malignant CA1a compared to AT1. These protein IDs are listed in Table 2 of Supporting Information. The higher level of expression of ribosome related proteins suggests increased translational activity in the malignant breast cancer cell line. One of these proteins, 60S ribosomal protein L14, was confirmed to be phosphorylated on Ser-138. No phosphorylation sites on this protein have previously been reported. When comparing the region of the RP chromatogram where this protein eluted (Fig. 8b), it can be seen that distinct and unique peak patterns are evident in both the CA1a and AT1 cell lines. L14 ribosomal protein was only identified in the CA1a cell line.

3.3.4 Mitosis

Malignant cells tend to have increased rates of mitosis due to their proliferative nature. Proteins involved in mitotic spindle formation appeared to be differentially phosphorylated between the two cell lines. One such protein, Stathmin (Op18) was uniquely phosphorylated in only the pre-malignant AT1. This protein regulates the microtubule filament system by destabilizing microtubule assembly.

Nuclear migration protein (NudC) and microtubule-associated protein (MAP4) are involved in correct formation of mitotic spindle. NudC is also involved in cytokinesis and cell proliferation. A higher expression of phosphorylated NudC could be indicative of the malignant nature of the CA1a cell line.

Heat shock protein β-1 is a stress related protein which is found in the cytoplasm but which colocalizes with mitotic spindles and migrates to the nucleus during stress. Increased phosphorylation of this protein in the malignant

cell line could act as a signal for localization to a particular part of the cell.

Nuclear envelope disintegration is an integral component of mitosis. Lamins provide a framework for the nuclear envelope and may also indirectly interact with chromatin. In both cell lines, different forms of lamin were confirmed to be phosphorylated by MS/MS. Lamins are known to be extensively phosphorylated prior to nuclear disintegration during the mitosis process. Six phosphorylation sites were found on lamin A/C in the CA1a malignant cell line, of which two had not been previously reported (S17 and S18). In addition, seven sites were found on lamin A/C in the premalignant AT1 cell line. Three of these sites were the same as the ones found in the CA1a cell line, while four were unique, of which one was predicted to be phosphorylated although no experimental evidence has been previously reported. Lamin phosphorylation is involved in regulation of lamin interactions making the differential phosphorylation of this protein between the two cell lines particularly noteworthy.

3.3.5 Enzymes

Few proteins involved in anabolic or catabolic enzymatic processes showed phosphorylation differences between AT1 and CA1a cells. However, two examples with relevance to cancer progression were aromatase and α-enolase. α-Enolase (MBP1) is a multifunctional enzyme playing a role in many processes, including glycolysis and growth control. When MPB1 binds to the c-myc promoter, it acts as a transcriptional repressor. α-Enolase has been implicated as a potential diagnostic marker for many cancers. In this study, MPB1 was identified in a phosphorylated form in only the AT1 cell line. Aromatase catalyzes the conversion of testosterone to estradiol. It has been reported that a kinase activity may be involved in the regulation of this catalytic process [42]. In this study, a phosphorylated form of aromatase was uniquely found in the premalignant AT1 cell line. It is plausible that phosphorylation of this enzyme renders it inactive. Consequently, the absence of estradiol in the premalignant AT1 may reduce the proliferative capability of the cell line.

3.3.6 Differential expression of proteins in p*I* range 7.0–6.6

Both the first and second dimension chromatograms suggested increased levels of protein in the higher pH separation range in the malignant CA1a cell line compared to the premalignant AT1 cell line. Proteins from the range 7.0–6.6 in the malignant CA1a cell line were analyzed and identified by MS/MS to see if this increase was specific to any particular class of proteins. Figure 9 shows a chromatogram of the second dimension separation in the 7.0–6.8 pH range. Interestingly, most identified proteins were ribosomal proteins and other proteins that regulate ribosomal function and genesis (shown in Table 2 of Supporting Information). A majority of the proteins identified are known to be phosphorylated and often times the presence or absence of phosphorylation determines their location or activation status in the cell. Furthermore, a large number of positive spots in the microarray (suggesting that the protein in the spot was phosphorylated) corresponded to the fractions analyzed in this high pH region. We were unable to locate the phosphorylation sites on all of these proteins, partly due to the low sequence coverage of most ribosomal proteins due to their low molecular weights. The theoretical isoelectric points of these ribosomal proteins are beyond the detection and separation capabilities of CF (between pH 8 and 11). It is likely that there appeared to be a higher expression of these proteins in the malignant CA1a because in fact these proteins were phosphorylated in the malignant cell line and therefore acquired a lower p*I* that made them detectable using the separation scheme used in these experiments.

4 Concluding remarks

The new hybrid approach presented here has significant advantages over classical 2-DE/MS/MS and 2-D LC MS/MS methods. Given the upfront enrichment of a specific class of proteins, the approach saves considerable time, both overall and with respect to MS instrument usage. The enrichment or selection of a subset of the total proteome enables the focused analysis of that class of protein without having to sequence and identify a majority of the proteome that may not be of interest for a specific study. Attempting to extract information on a subset of proteins from the total proteome is also less efficient because the proteins of interest may be diluted, or obscured by the majority. Furthermore, proteins of low abundance, or extreme p*I* or solubility characteristics are more likely to be detected and characterized in enriched samples. Thus, the method we describe here for the study of the phosphoproteome enables the identification of a broader range of phosphoproteins than conventional approaches.

A comparison of premalignant *versus* malignant breast cells has not been previously reported using the strategy described here. In summary, a total of 51 phosphorylation sites in 27 different proteins were confirmed using MS/MS and the status of these proteins was found to be specifically associated with the cellular phenotype. Forty-eight additional previously known phosphoproteins were identified without site confirmation. The ontological association of the differentially expressed phosphoproteins included mitosis, apoptosis suppression, and translational control. The research presented here illustrates the use of protein microarrays together with MS as complementary tools to study phosphoproteins in complex samples. The microarray is often able to detect the presence of phosphorylation not detected by MS without using enrichment techniques. When sample amounts are too low to permit enrichment the inability to detect phosphorylation by MS becomes a critical issue, making the protein microarray strategy a valuable alternative means of detecting high to medium abundance phospho-

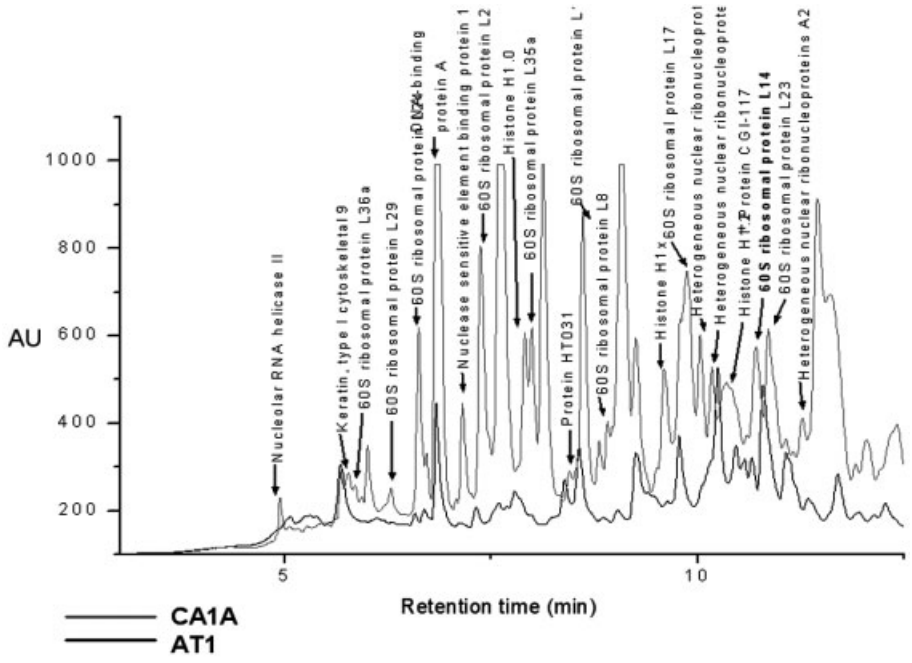

Figure 9. Comparison of RP chromatograms of pH fraction 7.0–6.8 from AT1 and CA1a to illustrate presence of larger amounts of transcriptional and translational regulatory proteins in malignant CA1a but not in premalignant AT1.

proteins which play a pivotal role in cellular phenotype. Site mapping by MS would subsequently be needed for complete characterization; however the strategy outlined above can be used as an effective and rapid initial screen.

We would like to thank Dr. David Misek of the University of Michigan for helpful suggestions and a critical reading of the manuscript. This work was supported in part by the National Cancer Institute under grant R01CA106402 (D.M.L.), R01CA90503 (FRM, D. M. L.), R01CA100104 (D. M. L.), and R01CA108597 (S. G.) and the National Institute of Health under grant RO1GM49500 (D. M. L.). T. H. P. received support under a Rackham PreDoctoral Fellowship and an Eastman Chemical Company summer fellowship.

The authors have declared no conflict of interest.

5 References

[1] American Cancer Society. *Breast Cancer Facts and Figures 2007–2008.* Atlanta: American Cancer Society, Inc.

[2] Wolf-Yadlin, A., Kumar, N., Zhang, Y., Hautaniemi, S. *et al.*, Effects of HER2 overexpression on cell signaling networks governing proliferation and migration. *Mol. Syst. Biol.* 2006, *2*, 54.

[3] Yu, Y., Hao, Y., Feig, L. A., The R-Ras GTPase mediates cross talk between estrogen and insulin signaling in breast cancer cells. *Mol. Cell. Biol.* 2006, *26*, 6372–6380.

[4] Hunter, T., The role of tyrosine phosphorylation in cell growth and disease. *Harvey Lect.* 1998, *94*, 81–119.

[5] Chow, S., Minden, M. D., Hedley, D. W., Constitutive phosphorylation of the S6 ribosomal protein via mTOR and ERK signaling in the peripheral blasts of acute leukemia patients. *Exp. Hematol.* 2006, *34*, 1183–1191.

[6] Spickett, C. M., Pitt, A. R., Morrice, N., Kolch, W., Proteomic analysis of phosphorylation, oxidation and nitrosylation in signal transduction. *Biochim. Biophys. Acta* 2006, *1764*, 1823–1841.

[7] Cohen, P., The role of protein phosphorylation in human health and disease. The Sir Hans Krebs Medal Lecture. *Eur. J. Biochem.* 2001, *268*, 5001–5010.

[8] Perkins, N. D., Post-translational modifications regulating the activity and function of the nuclear factor kappa B pathway. *Oncogene* 2006, *25*, 6717–6730.

[9] Krueger, K. E., Srivastava, S., Posttranslational protein modifications: Current implications for cancer detection, prevention, and therapeutics. *Mol. Cell. Proteomics* 2006, *5*, 1799–1810.

[10] Morandell, S., Stasyk, T., Grosstessner-Hain, K., Roitinger, E. *et al.*, Phosphoproteomics strategies for the functional analysis of signal transduction. *Proteomics* 2006, *6*, 4047–4056.

[11] Yu, L. R., Issaq, H. J., Veenstra, T. D., Phosphoproteornics for the discovery of kinases as cancer biornarkers and drug targets. *Proteomics Clin. Appl.* 2007, *1*, 1042–1057.

[12] Tavares, A., Cimarosti, H., Valentim, L., Salbego, C., Profile of phosphoprotein labelling in organotypic slice cultures of rat hippocampus. *Neuroreport* 2001, *12*, 2705–2709.

[13] Kaufmann, H., Bailey, J. E., Fussenegger, M., Use of antibodies for detection of phosphorylated proteins separated by two-dimensional gel electrophoresis. *Proteomics* 2001, *1*, 194–199.

[14] Goodman, T., Schulenberg, B., Steinberg, T. H., Patton, W. F., Detection of phosphoproteins on electroblot membranes

using a small-molecule organic fluorophore. *Electrophoresis* 2004, *25*, 2533–2538.

[15] Martin, K., Steinberg, T. H., Goodman, T., Schulenberg, B. *et al.*, Strategies and solid-phase formats for the analysis of protein and peptide phosphorylation employing a novel fluorescent phosphorylation sensor dye. *Comb. Chem. High Throughput Screen.* 2003, *6*, 331–339.

[16] Steinberg, T. H., Agnew, B. J., Gee, K. R., Leung, W. Y. *et al.*, Global quantitative phosphoprotein analysis using multiplexed proteomics technology. *Proteomics* 2003, *3*, 1128–1144.

[17] Martin, K., Steinberg, T. H., Cooley, L. A., Gee, K. R. *et al.*, Quantitative analysis of protein phosphorylation status and protein kinase activity on microarrays using a novel fluorescent phosphorylation sensor dye. *Proteomics* 2003, *3*, 1244–1255.

[18] McDonald, T., Sheng, S., Stanley, B., Chen, D. *et al.*, Expanding the subproteome of the inner mitochondria using protein separation technologies: One- and two-dimensional liquid chromatography and two-dimensional gel electrophoresis. *Mol. Cell. Proteomics* 2006, *5*, 2392–2411.

[19] Sheng, S., Chen, D., Van Eyk, J. E., Multidimensional liquid chromatography separation of intact proteins by chromatographic focusing and reversed phase of the human serum proteome: Optimization and protein database. *Mol. Cell. Proteomics* 2006, *5*, 26–34.

[20] Billecke, C., Malik, I., Movsisyan, A., Sulghani, S. *et al.*, Analysis of glioma cell platinum response by metacomparison of two-dimensional chromatographic proteome profiles. *Mol. Cell. Proteomics* 2006, *5*, 35–42.

[21] Skalnikova, H., Halada, P., Dzubak, P., Hajduch, M., Kovarova, H., Protein fingerprints of anti-cancer effects of cyclin-dependent kinase inhibition: Identification of candidate biomarkers using 2-D liquid phase separation coupled to mass spectrometry. *Technol. Cancer Res. Treat.* 2005, *4*, 447–454.

[22] Cantin, G. T., Yates, J. R., III, Strategies for shotgun identification of post-translational modifications by mass spectrometry. *J. Chromatogr. A* 2004, *1053*, 7–14.

[23] Cantin, G. T., Venable, J. D., Cociorva, D., Yates, J. R., III, Quantitative phosphoproteomic analysis of the tumor necrosis factor pathway. *J. Proteome Res.* 2006, *5*, 127–134.

[24] MacCoss, M. J., McDonald, W. H., Saraf, A., Sadygov, R. *et al.*, Shotgun identification of protein modifications from protein complexes and lens tissue. *Proc. Natl. Acad. Sci. USA* 2002, *99*, 7900–7905.

[25] Andersson, L., Porath, J., Isolation of phosphoproteins by immobilized metal (Fe3+) affinity chromatography. *Anal. Biochem.* 1986, *154*, 250–254.

[26] Ndassa, Y. M., Orsi, C., Marto, J. A., Chen, S., Ross, M. M., Improved immobilized metal affinity chromatography for large-scale phosphoproteomics applications. *J. Proteome Res.* 2006, *5*, 2789–2799.

[27] Kweon, H. K., Hakansson, K., Selective zirconium dioxide-based enrichment of phosphorylated peptides for mass spectrometric analysis. *Anal. Chem.* 2006, *78*, 1743–1749.

[28] Nesvizhskii, A. I., Protein identification by tandem mass spectrometry and sequence database searching. *Methods Mol. Biol.* 2007, *367*, 87–119.

[29] Schabacker, D. S., Stefanovska, I., Gavin, I., Pedrak, C., Chandler, D. P., Protein array staining methods for undefined protein content, manufacturing quality control, and performance validation. *Anal. Biochem.* 2006, *359*, 84–93.

[30] Pal, M., Moffa, A., Sreekumar, A., Ethier, S. P. *et al.*, Differential phosphoprotein mapping in cancer cells using protein microarrays produced from 2-D liquid fractionation. *Anal. Chem.* 2006, *78*, 702–710.

[31] Dawson, P. J., Wolman, S. R., Tait, L., Heppner, G. H., Miller, F. R., MCF10AT: A model for the evolution of cancer from proliferative breast disease. *Am. J. Pathol.* 1996, *148*, 313–319.

[32] Miller, F. R., Xenograft models of premalignant breast disease. *J. Mammary Gland Biol. Neoplasia* 2000, *5*, 379–391.

[33] Santner, S. J., Dawson, P. J., Tait, L., Soule, H. D. *et al.*, Malignant MCF10CA1 cell lines derived from premalignant human breast epithelial MCF10AT cells. *Breast Cancer Res. Treat.* 2001, *65*, 101–110.

[34] Stasyk, T., Morandell, S., Bakry, R., Feuerstein, I. *et al.*, Quantitative detection of phosphoproteins by combination of two-dimensional difference gel electrophoresis and phosphospecific fluorescent staining. *Electrophoresis* 2005, *26*, 2850–2854.

[35] Godovac-Zimmermann, J., Soskic, V., Poznanovic, S., Brianza, F., Functional proteomics of signal transduction by membrane receptors. *Electrophoresis* 1999, *20*, 952–961.

[36] Zhu, K., Zhao, J., Lubman, D. M., Miller, F. R., Barder, T. J., Protein p*I* shifts due to posttranslational modifications in the separation and characterization of proteins. *Anal. Chem.* 2005, *77*, 2745–2755.

[37] Datta, S. R., Ranger, A. M., Lin, M. Z., Sturgill, J. F. *et al.*, Survival factor-mediated BAD phosphorylation raises the mitochondrial threshold for apoptosis. *Dev. Cell* 2002, *3*, 631–643.

[38] Sastry, K. S., Smith, A. J., Karpova, Y., Datta, S. R., Kulik, G., Diverse antiapoptotic signaling pathways activated by vasoactive intestinal polypeptide, epidermal growth factor, and phosphatidylinositol 3-kinase in prostate cancer cells converge on BAD. *J. Biol. Chem.* 2006, *281*, 20891–20901.

[39] Xin, M., Deng, X., Nicotine inactivation of the proapoptotic function of Bax through phosphorylation. *J. Biol. Chem.* 2005, *280*, 10781–10789.

[40] Kim, B. J., Ryu, S. W., Song, B. J., JNK- and p38 kinase-mediated phosphorylation of Bax leads to its activation and mitochondrial translocation and to apoptosis of human hepatoma HepG2 cells. *J. Biol. Chem.* 2006, *281*, 21256–21265.

[41] Hu, Y., Yao, J., Liu, Z., Liu, X. *et al.*, Akt phosphorylates acinus and inhibits its proteolytic cleavage, preventing chromatin condensation. *EMBO J.* 2005, *24*, 3543–3554.

[42] Balthazart, J., Baillien, M., Ball, G. F., Phosphorylation processes mediate rapid changes of brain aromatase activity. *J. Steroid Biochem. Mol. Biol.* 2001, *79*, 261–277.

